ELSEVIER

Earth and Planetary Science Letters 154 (1998) 93–107

EPSL

Incision and differential bedrock uplift along the Indus River near Nanga Parbat, Pakistan Himalaya, from ^{10}Be and ^{26}Al exposure age dating of bedrock straths

J. Leland [a,*], M.R. Reid [a], D.W. Burbank [b,1], R. Finkel [c], M. Caffee [c]

[a] *W.M. Keck Foundation Center for Isotope Geochemistry, Department of Earth and Space Sciences, University of California, Los Angeles, CA 90095-1567, USA*

[b] *Department of Earth Sciences, University of Southern California, Los Angeles, CA 90089-0740, USA*

[c] *Institute of Geophysics and Planetary Physics / Center for Accelerator Mass Spectrometry, Lawrence Livermore National Laboratory, 7000 East Avenue, Livermore, CA 94550, USA*

Received 23 May 1997; accepted 22 September 1997

Abstract

Well preserved, river-cut bedrock surfaces (straths) abandoned by the progressive incision of the Indus River in northern Pakistan were dated using in situ cosmogenic ^{10}Be and ^{26}Al exposure age dating. Measurements on young and modern straths show no significant ingrowth of ^{10}Be and ^{26}Al, implying that strath exposure ages closely approximate their abandonment age. Strath exposure ages range up to 65 ka and increase with height above the river. The straths can be divided into two groups: low straths dated at about 7 ka, which yield very rapid bedrock incision rates (9–12 m/ka), and high straths > 7 ka in age, which yield somewhat slower incision rates (1–6 m/ka). Incision rates for both groups increase by ~ 1–3 m/ka downstream toward an active reverse fault, the Raikot fault, that forms the western border of the Nanga Parbat–Haramosh massif (NPHM). The downstream increases in incision rates for the low straths mimic downstream increases in the modern gradient, suggesting that bedrock incision rates have been proportional to stream power over the last 7 ka. Gradient increases are probably the result of the creation of knickpoints by bedrock uplift along the Raikot fault. The longitudinal profile and steep gorge of the Indus River in the study area indicate that bedrock incision appears to keep pace with differential vertical motions between the NPHM and surrounding regions. Thus, the 1–3 m/ka difference in incision rates likely reflects the differential bedrock uplift rate between the NPHM and the Skardu Basin. The differential incision rate is consistent with differential exhumation rates obtained from apatite fission track ages assuming geotherms of ≤ 80–90°C/km in the NPHM and 35°C/km in the Skardu Basin. This relation suggests that rapid bedrock incision of at least 1–3 m/ka has persisted within the NPHM for the last 0.5 Ma. The acceleration of incision rates throughout the study area since 15 ka is likely to be a climatic signal that records an increase in the discharge and/or sediment load of the Indus River in the study area related to deglaciation of the surrounding terrane. © 1998 Elsevier Science B.V.

Keywords: Indus River; erosion rates; exposure age; Be-10; Al-26; uplifts

* Corresponding author. Tel.: +1 310 825 3241. Fax: +1 310 825 2779. E-mail: leland@ess.ucla.edu

[1] Present address: Department of Geosciences, Pennsylvania State University, University Park, PA 16802, USA.

PII S0012-821X(97)00171-4

1. Introduction

Streams interact with the landscape through a complex system of feedbacks involving climate, topography, and tectonics. In an active alpine belt, the relative contributions of these influences can be at least partially unravelled through knowledge of the temporal variation in the gradient, discharge, and load of one or more major streams draining the area. Longitudinal profile histories can be constructed from abandoned stream terraces; from these, gradient-related effects on past stream power can be estimated. Rates of fluvial incision through bedrock, an elusive measurement until recently [1–3], can be used to constrain the magnitude of a stream's ability to contribute to denudation of the landscape and respond to external tectonic forcing (e.g., [4]). In this study, we use exposure age dating of river-cut terraces to reconstruct paleo-profiles and to quantify bedrock incision rates along the Indus River in a tectonically active region of northern Pakistan.

In northern Pakistan (Fig. 1A), the Indus River flows through a spectacular mountain landscape confined within the steep-walled Middle Gorge (MG) between the Himalaya and Karakoram mountain ranges. In the MG the Indus River flows on crystalline bedrock with a steep average gradient of about 5 m/km [5] from the Skardu Basin, a roughly 400 km^2 basin in the east, to the confluence with the Gilgit River to the west (Fig. 1A). Near the western end of the MG, the Indus River crosses the Nanga Parbat–Haramosh massif (NPHM), a region characterized by some of the highest mountains in northern Pakistan and bounded on the west by the Raikot fault zone, a complex of active faults with both strike-slip and reverse motion indicators [6]. The relief between the river and the top of Nanga Parbat in the NPHM is almost 7000 m and exposes Indian plate basement gneisses (Fig. 1A) that form the northwestern syntaxis of the Himalaya. Within the NPHM the river's gradient steepens to about 7 m/km [5]. Apatite fission track ages [7] are youngest in the Indian plate basement gneisses of the NPHM, rapidly increase to the east and west (Fig. 1B), and indicate that exhumation rates between the Skardu Basin and the NPHM could differ by as much as an order of magnitude.

The active reverse fault, steepening of the river's gradient, and young fission track ages in the NPHM suggest that this area is experiencing more rapid bedrock uplift rates with respect to regions upstream and that it has been doing so for > 1 Ma. If true, the maintenance of a downstream gradient requires that the confined Indus River must either be incising more rapidly within the NPHM compared to points immediately upstream or aggrading upstream. To quantify the magnitude and variation in incision along the Indus River in the MG, we obtained cosmic ray exposure ages, using cosmogenic ^{10}Be and ^{26}Al, for bedrock, river-cut terraces preserved in the MG (cf. [5]). These river-cut terraces, or straths, are remnant river bottoms abandoned by the Indus River as it progressively incised into the deeper portions of its bedrock channel. Exposure age dating of these straths yields the time that has elapsed since their abandonment by the Indus River. The MG is an ideal place to examine incision rate changes related to tectonic rejuvenation because, within the MG, there are no significant additions to discharge and the Indus River's channel is floored by hard, resistant material (Fig. 1A and Table 1).

This paper presents a larger and more precise data set than our preliminary results [5]. These new data show that, for the past 7 ka, bedrock incision rates have been even higher than those we reported previously [5]. Despite the late Quaternary acceleration in incision rates with time, a consistent difference in incision rate between the NPHM and upper reaches of the MG near the Skardu Basin is maintained, but this difference (1–3 m/ka) is less than previously inferred (5–10 m/ka). Stream paleo-profiles suggest a previously unrecognized climatic influence, as well as tectonic controls on incision rates. When patterns of incision rates are considered together with longer term exhumation rates, inferred from apatite fission track ages [7], relative rates of bedrock uplift in the NPHM are deduced to be 3–4 m/ka greater than those upstream, comparable to values obtained in [5].

2. Field observations

Strath distribution is irregular throughout the MG of the Indus River and straths are rare in the NPHM, where exhumation rates are highest. They are usually

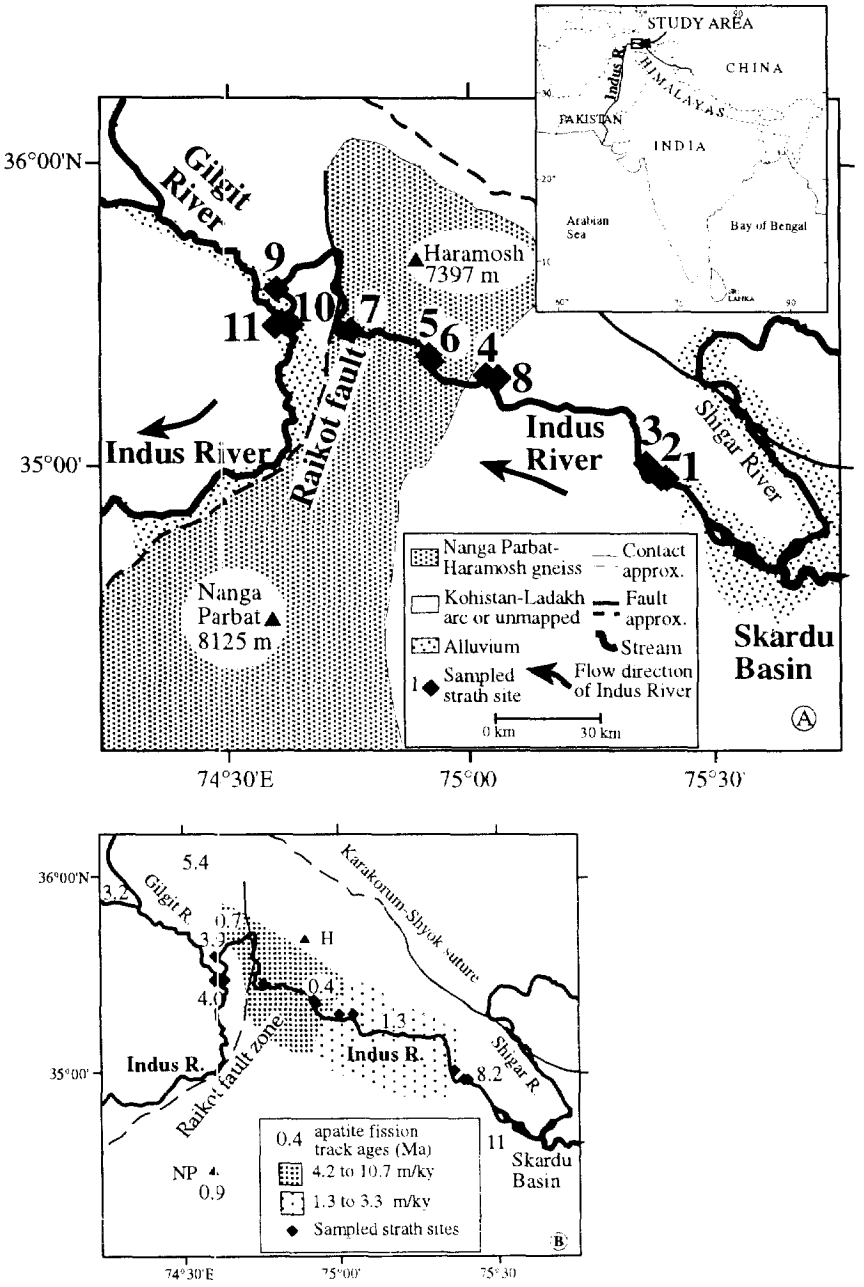

Fig. 1. (A) Geologic map (based on [22,33]) of the study area showing the location of numbered strath sites. Arrows show the direction of flow in the Indus River. Relief between the Indus River and surrounding mountain peaks is up to 7000 m. The active Raikot fault zone is probably accommodating both reverse and strike-slip motions along the western side of the Nanga Parbat–Haramosh massif (NPHM) [6]. Inset shows the regional location of the Middle Gorge (MG) of the Indus River in northern Pakistan. (B) Map showing distribution of apatite fission track ages [7], the youngest of which occur within the shaded region defining an axis of rapid exhumation within the NPHM. The range of exhumation rates reported are for the ages nearest the river and assume two bounding geotherms of 35 and 90°C/km and a 150°C closure temperature for apatite [24]. Using the steeper geotherm, exhumation rates increase 2.9 m/ka between the two shaded regions, a value that is similar to the downstream increase in incision rates.

Table 1
Sample descriptions

Strath #	Lat. (°N)	Long. (°E)	Sample ID	Altitude (km)	Block angle (°)	Depth (cm)	Rock type
1	35.48	75.40	PK93-20	2.235	29	1.0	garnet sillimanite biotite q-f schist
			PK93-21	2.233	27	2.0	garnet sillimanite biotite q-f schist
			PK93-22	2.233	31	1.0	garnet sillimanite biotite q-f schist
2	35.48	75.39	PK93-23	2.198	29	3.0	amphibole biotite q-f schist
			PK93-24	2.198	29	3.0	amphibole biotite q-f schist
			PK93-25	2.195	29	5.0	quartz vein in schist
3	35.51	75.35	PK93-17	2.082	26	1.0	garnet two mica q-f schist
			PK93-19	2.082	26	1.3	garnet two mica q-f schist
4a	35.63	75.02	PK93-94	1.802	34	5.0	garnet biotite q-f schist
4b	35.63	75.02	PK93-35	1.822	47	1.5	garnet biotite q-f schist
4c	35.63	75.02	PK93-29	1.850	29	2.5	garnet biotite q-f schist
			PK93-30	1.845	29	3.0	garnet biotite q-f schist
5	35.67	74.92	PK95-31	2.138	24	1.0	kyanite biotite q-f gneiss
			PK95-32	2.138	24	2.0	kyanite biotite q-f gneiss
6a	35.67	74.92	PK95-29	1.729	37	4.0	kyanite biotite q-f gneiss
			PK95-30	1.728	37	4.0	kyanite biotite q-f gneiss
6b	35.67	74.92	PK93-36	1.883	27	1.0	kyanite biotite q-f gneiss
			PK93-37	1.883	27	1.0	kyanite biotite q-f gneiss
			PK93-38	1.882	28	1.0	kyanite biotite q-f gneiss
7	35.71	74.75	PK93-39	1.675	31	2.0	sillimanite biotite q-f gneiss
			PK93-40	1.675	31	0.8	sillimanite biotite q-f gneiss
8	35.63	75.06	PK95-19	2.009	26	0.5	foliated biotite granodiorite
			PK95-21	1.981	26	3.0	stretched q-f pegmatite
9	35.78	74.63	PK95-12	1.372	31	3.5	biotite granodiorite
			PK95-13	1.372	31	1.5	biotite granodiorite
10	35.72	74.65	PK93-52	1.355	20	2.5	tourmaline leuco-granite
			PK93-53	1.355	15	3.0	tourmaline leuco-granite
11	35.72	74.63	PK95-8	1.311	19	2.0	biotite granodiorite
			PK95-9	1.314	19	1.5	biotite granodiorite

unpaired and some are located near the confluences of small tributaries with the Indus River. Straths are most common several tens of meters above the modern river and become less frequent at higher levels. At levels > 100 m above the river, sampled straths range from approximately 10 to 20 m wide and 30 to 100 m long; lower straths tend to be broader and longer than higher straths.

The strath surfaces commonly consist of well rounded bedrock knobs from 1 to 30 m in height as well as flatter, planated areas of variable width. All surfaces display fluvial features, such as sculpted flutes, potholes, and smooth polish, comparable to those found within the modern bedrock channel of the Indus River. Fig. 2 illustrates an abandoned strath 70 m above the river level.

Higher straths are affected by differential weathering. These strath surfaces preserve patches of fluvially sculpted and polished bedrock adjacent to degraded surfaces which retain evidence of fluvial sculpting (fluting, rounded edges and potholes) but lack extensive polish or smoothness. In addition, desert varnish development to depths of 1 mm is ubiquitous on well preserved surfaces and patchy to non-existent on hackly, degraded portions of the higher straths. Degraded surfaces are usually located near drainage points off the surface or in low areas where soil formation has begun.

3. Sampling and analytical methods

3.1. Field sampling

Samples for cosmogenic exposure age dating were collected from strath terraces throughout the MG

Fig. 2. The strath at site 6b, 70 m above the Indus, shows remarkable preservation of fluvial sculpting. The right margin of the photograph shows a low area covered with cryptogam, a mossy-feeling symbiosis of fungus and licher that traps dust and moisture, the type of area avoided during sampling.

(Fig. 1A). Samples listed in Table 1 are grouped by strath number according to their location along the river. Numbered strath sites with multiple terraces are further distinguished by the use of a lower case letter next to the strath number. We attempted to avoid sampling straths near landslides and chose straths that were protected from adjacent hillslope debris flows by bedrock buttresses. A landslide deposit occurs 70 m behind and 30 m above strath 3 but no debris is currently present at the site. Straths 9–11 are located near or at the confluence between the Gilgit and Indus Rivers where the channel widens and both discharge and gradient change; 9 and 10 are mantled or stratigraphically sandwiched between fill terraces and may have experienced more complex exposure histories than straths 1–8.

^{10}Be and ^{26}Al production varies as a function of latitude, altitude, depth, and exposure angle [8,9] and these variables were carefully quantified (Table 1). Sampled strath terraces were located using both published topographic maps and images rendered from a 3 arcsecond ($\sim$ 90 m grid) digital elevation database. The sampled terraces were also pinpointed using GPS whenever possible. The elevations of the terraces and the river bank immediately below were recorded using a barometric altimeter in a closed loop to adjust for instrument drift. The estimated error in the relative determination of elevation between terrace and nearby river bank is 6 m; for lower straths and other small elevation differences, the estimated error is lessened by visual inspection to 1 m. Cosmic ray blocking angles were surveyed at each sample site along eight compass points to correct production rates for exposure geometry [8].

3.2. Sample preparation and analyses

Quartz was separated from the collected samples so that empirically measured in situ production rates of ^{10}Be and ^{26}Al in quartz [8] could be applied for dating. Measurements typically required 10–40 g of pure quartz separated from at least 150 g of starting material with $>$ 15% modal quartz. Bulk samples were coarsely crushed with a steel mortar and pestle, and an aliquot was finely crushed to a size (typically 45–250 μm) that maximized the number of monominerallic grains in the split without powdering the sample. Magnetic separation served to concentrate the felsic fraction. Quartz was purified and leached to eliminate meteoric ^{10}Be from the felsic fractions using the protocol described in [10]. For those felsic fractions containing impurities, such as garnet or kyanite, heavy liquid separations using methylene iodide and acetone were employed midway through the leaching process. This technique was repeated until the Al concentration was $<$ 1000 ppm. For approximately a quarter of the quartz fractions, tiny inclusions of aluminosilicates such as sillimanite, kyanite, and garnet defied all separation efforts, resulting in samples with ^{26}Al/^{27}Al below detection limits.

Table 2
^{10}Be and ^{26}Al results for straths along the Middle Gorge of the Indus River, Pakistan

Strath #	Sample ID	Height[a] (m)	^{10}Be/^{9}Be[b] (10^{-15})	2σ (10^{-15})	^{10}Be conc. (10^{6} at/g)	2σ (10^{6} at/g)	^{10}Be age[c] (ka)	2σ (ka)	Max ε[d] (m/ka)	^{26}Al/^{27}Al[b] (10^{-15})	2σ (10^{-15})	^{26}Al (10^{6} at/g)	2σ (10^{6} at/g)	^{26}Al age (ka)	2σ (ka)	Max ε[d] (m/ka)	Al/Be (norm[e])	2σ	Av. strath age[f] (ka)	2σ (ka)
1	PK93-20-1B	185	605.8	66.0	1.299	0.142	55.0	6.1	0.0106								56.1	5.8		
	PK93-21-1	183	*746.0*	*52.8*	*0.857*	*0.068*	*35.6*	*2.8*	*0.0164*	*473.5*	*50.4*	*4.455*	*0.482*	*30.8*	*3.3*	*0.0189*	*5.24*	*0.70*		
	PK93-22-1A	183	401.0	110.0	1.532	0.421	66.8	18.6	0.0087											
2	PK93-23-1	148	844.8	76.5	1.487	0.138	65.4	6.0	0.0089	2706.0	198.0	9.243	0.701	68.4	5.0	0.0083	6.26	0.75	65.0	2.4
	PK93-24-1A	148	909.7	52.8	1.452	0.088	63.9	3.9	0.0091	4016.0	300.1	8.557	0.675	63.2	5.0	0.0091	5.94	0.59		
	PK93-25-1A1	145	*490.7*	*33.2*	*0.744*	*0.053*	*33.1*	*2.3*	*0.0177*											
	PK93-25-1A	145	*631.0*	*40.0*	*0.754*	*0.049*	*33.6*	*2.2*	*0.0174*	*5447.0*	*620.0*	*4.371*	*0.522*	*32.4*	*3.9*	*0.0179*	*5.84*	*0.80*		
3	PK93-17-1A	65	85.0	13.2	0.146	0.023	6.6	1.0	0.0898	34.2	28.9	0.698	0.589	5.2	4.4	0.114	4.81	4.13	6.8	0.8
	PK93-19-1A	65	139.9	30.0	0.174	0.038	7.8	1.7	0.0753	41.8	12.8	0.918	0.281	6.8	2.1	0.0862	5.32	1.99		
4a	PK93-34-1	22	38.4	15.4	0.043	0.017	2.6	1.1	0.226	441.4	200.0	0.272	0.124	2.7	1.2	0.216	6.36	3.86	2.7	1.0
4b	PK93-35-1	42	18.0	10.4	0.033	0.019	2.5	1.4	0.238										2.5	1.4
4c	PK93-29-1AB	70	65.2	16.0	0.125	0.031	6.8	1.7	0.0863										5.9	1.1
	PK93 30 1B	65								12.8										
	PK93-30-1AB	65	43.2	12.9	0.103	0.031	5.7	1.7	0.1040											
5	PK95-31-1A	410	455.3	35.2	0.763	0.060	32.3	2.6	0.0181	261.1	36.5	4.499	0.654	31.6	4.6	0.0183	5.94	0.98	32.2	2.0
	PK95-31-1A	410								269.7	38.0	4.647	0.681	32.7	4.8	0.0177				
	PK95-32-1A1	410	*242.8*	*18.6*	*0.326*	*0.028*	*13.8*	*1.2*	*0.0424*	*177.3*	*24.0*	*1.940*	*0.275*	*13.6*	*1.9*	*0.0429*	*5.99*	*0.99*		
6a	PK95-29-1A	2	46.9	17.8	0.047	0.018	3.1	1.2	0.190	1.0	3.0	0.009	0.029	0.1	0.3	5.84	0.20	0.62	0.2	0.2
	PK95-30-1A	1	5.1	8.4	0.006	0.010	0.4	0.7	1.48	0.1	3.0	0.001	0.041	0.0	0.5	49.6	0.18	6.90		
6b	*PK93-36-1B*	155	*68.7*	*38.0*	*0.235*	*0.130*	*12.1*	*6.7*	*0.0487*	*113.3*	*24.0*	*1.699*	*0.361*	*14.4*	*3.1*	*0.0405*	*7.26*	*4.31*	*27.1*	*2.6*
	PK93-37-1A	155	*243.9*	*20.0*	*0.235*	*0.020*	*12.1*	*1.0*	*0.0487*	*76.2*	*10.2*	*1.419*	*0.190*	*12.1*	*1.6*	*0.0486*	*6.07*	*0.97*		
	PK93-38-1A	154	252.5	22.0	0.547	0.050	28.5	2.6	0.0205	417.6	46.0	2.926	0.326	25.3	2.8	0.0230	5.39	0.77		
7	PK93-39-1AB	80	95.4	17.2	0.128	0.023	8.0	1.5	0.0736										6.7	0.9
	PK93-40-1AB	80	70.8	14.7	0.094	0.020	5.8	1.2	0.1012											
8	PK95-19-1A	192	651.0	70.0	0.826	0.090	38.7	4.2	0.0151	2994.0	172.0	5.088	0.305	39.8	2.4	0.0145	6.21	0.77	41.3	1.5
	PK95-21-1A	164	738.1	34.0	0.875	0.043	42.7	2.1	0.0137	25090.0	5600.0	8.694	1.942	71.8	16.0	0.0079	10.0	2.29		
9	PK95-12-1A	75	170.2	12.6	0.143	0.013	11.0	1.0	0.0533	994.2	126.0	0.904	0.117	11.5	1.5	0.0508	6.36	0.99	11.0	0.6
	PK95-13-1	75	92.0	8.4	0.132	0.014	10.1	1.0	0.0585	2795.0	360.0	0.976	0.126	12.2	1.6	0.0479	7.41	1.23		
10	PK93-52-1A	105	166.0	17.5	0.132	0.015	9.4	1.0	0.0627	1008.0	200.1	0.848	0.168	10.0	2.0	0.0589	6.46	1.47	9.5	0.9
	PK93-53-1A	105	*89.8*	*11.6*	*0.082*	*0.011*	*5.7*	*0.8*	*0.1025*	*557.6*	*70.0*	*0.390*	*0.049*	*4.5*	*0.6*	*0.130*	*4.80*	*0.87*		
11	PK95-8-1A	61	100.0	10.6	0.099	0.012	7.2	0.9	0.0817	989.5	220.0	0.550	0.125	6.6	1.5	0.0890	5.58	1.43	7.2	0.5
	PK95-9-1A	64	120.0	11.8	0.104	0.011	7.5	0.8	0.0781	384.1	134.0	0.552	0.193	6.6	2.3	0.0893	5.32	1.94		
	Column Blank		6.5	4.0						3.0	2.9									

[a] Elevation above local river level.
[b] Blank corrected ratios (excepting the column blank).
[c] All ages are calculated for the zero erosion case and are minimum ages ($\lambda^{10}\mathrm{Be} = 4.62 \times 10^{-7}\ \mathrm{a}^{-1}$, $\lambda^{26}\mathrm{Al} = 9.68 \times 10^{-7}\ \mathrm{a}^{-1}$; [34]).
[d] Maximum erosion rates are calculated for single isotopes by assuming infinite age [9].
[e] Values normalized to sea level and latitude > 60°.
[f] Values are weighted averages of ages in plain type. Italicized ages were excluded, as explained in the text.

Our Be–Al separation procedure began with the quantitative addition of low $^{10}Be/^{9}Be$ carrier (and low $^{26}Al/^{27}Al$ carrier for low Al samples) to a known quantity of the quartz mineral separate. The quartz was then completely dissolved in a 4:1 HF:HNO_3 solution, dried, redissolved in 2 N HCl, and the resulting solution was weighed. Total Al and Be concentrations were determined on a small aliquot of this solution using ion coupled plasma (ICP) emission spectroscopy. Analytical uncertainties are based on counting statistics over three 10 sec counting intervals. The additional uncertainty arising from the dilution factor for the analyte is $< 1\%$.

The 2 N HCl solution was evaporated and the precipitates were redissolved in 3.6 N HF and loaded on 20 ml capacity anion (Dowex 1-X8, 100–200 mesh, in F^- form) columns. Al was usually eluted in the fourth to sixth column volume and Be in the ninth to twelfth column volume. The appropriate column fractions were then dried down and treated with HNO_3 and NH_4OH in a series of washes. The purified Be and Al were loaded in small quartz vials, dried, and oxidized prior to loading in target holders for accelerator mass spectrometric (AMS) analysis. This separation procedure produces Be and Al that yield high, stable currents on the AMS. It effectively excludes B from the Be-bearing column fractions, thereby reducing isobaric (^{10}B) interferences during AMS analysis. The procedure also has a low probability for cross contamination between samples if the columns are properly washed and conditioned prior to use.

All $^{10}Be/^{9}Be$ and $^{26}Al/^{27}Al$ measurements were performed at the Lawrence Livermore National Laboratory Center for Accelerator Mass Spectrometry. Our carrier and column blanks averaged 6.5×10^{-15} for $^{10}Be/^{9}Be$ and 3.0×10^{-15} for $^{26}Al/^{27}Al$. Uncertainties for the blank-corrected AMS measurements (Table 2) are calculated from the analytical uncertainties associated with both the unknown and the reference standards, and assume a 30% uncertainty in the magnitude of the blank and isobaric interference corrections. The cosmogenic nuclide concentrations presented in Table 2 are the product of $^{10}Be/^{9}Be$ or $^{26}Al/^{27}Al$ and the Be or Al concentration of the sample. Calculated uncertainties in the ^{10}Be and ^{26}Al concentrations include the propagated uncertainties in both the AMS and ICP measurements. In all cases, the uncertainties from AMS measurements dominate the overall uncertainty in the reported nuclide concentration; in some cases, low signal strength resulted in large uncertainties.

The reproducibility of our analytical methods and measurements was tested. Two separate whole rock splits of PK93-25, 1A and 1A1, were processed at different times as described above. The resulting ^{10}Be concentrations, determined from AMS and ICP measurements run months apart, are listed in Table 2 and differ by less than 2%. $^{26}Al/^{27}Al$ AMS measurements taken several months apart on aliquots from the same Al fraction of PK95-31-1A differed by less than 5% (Table 2).

4. Results

4.1. Calculation of exposure ages and erosion rates

^{10}Be and ^{26}Al concentrations were measured in 32 different samples from 14 different terraces at 11 sites along the river (Table 2). Twelve of the 14 dated terraces are represented by two or more samples. Calculated exposure ages assume no post-abandonment erosion of the straths; because of the aridity of the area, snow cover is assumed to be negligible. We used production rates in quartz [8] corrected for the sample latitude and altitude [9], sample thickness, and sample exposure geometry using a 2π steradian, $\sin^{2.3}\theta$ distribution for cosmic rays [8], where θ is the angle from the horizon. Errors introduced into the calculated age by the geometric correction are likely to be less than 5% based on an estimated maximum error in average blocking angle of $\pm 5°$, given the relatively smooth variation in the blocking profile from one hemiquadrant to the next and the relative insensitivity of the calculation to changes in blocking angles between 0 and 30°, the range of most measured blocking angles (Table 1). Maximum post-abandonment erosion rates were calculated for each isotope using a constant erosion rate model with the absorption coefficient, μ, equal to 0.019 cm^{-1}, a rock density of 2.8 g cm^{-3}, and a cosmic ray attenuation factor for neutrons in rock of 150 g cm^{-2} [9].

We did not include the fundamental uncertainties in production rates, perhaps as high as 20% [9,11], in the errors on the ages. However, several factors

serve to minimize the absolute errors associated with applying production rates from Sierran Nevada quartz [8] to samples from the MG. Firstly, error in extrapolating production rates for altitude and latitude is minimized because the latitude (35.5°N) and the altitudes (1355–2235 m a.s.l.) of the sampled straths within the MG are similar to or lower than the latitude (37.5°N) and the altitudes (2060–3558 m a.s.l.) of the sampling sites for the production rate study in the Sierra Nevada [8,11]. Secondly, using those production rates for MG samples spanning 0 to 70 ka introduces dating errors that are likely to be no greater than 10%, despite changes in the geomagnetic field intensity [11]. Finally, the Sierran Nevadan production rates, which integrate changes over the last 11 ka, agree with production rates calculated from ^{10}Be and ^{26}Al concentrations measured in several samples from Meteor Crater, Arizona [12] and the 49 ka age of the site based on thermoluminescence in shocked quartz [13]. Thus, the available data suggest that the use of a constant production rate based on the Sierra Nevada study will probably introduce no more than a 10% uncertainty in the exposure ages of the MG surfaces. However, the exposure ages we calculate from the data are subject to change as the variations in and absolute values of production rates are better documented in the future.

4.2. Duration of strath formation

For exposure ages to date abandonment of the straths, surfaces exposed in bedrock straths must form quickly and not acquire a significant cosmogenic signature prior to their abandonment. To quantify the magnitude of cosmogenic nuclide accumulation during incision, ^{10}Be and ^{26}Al were measured in two samples collected from an actively forming, fluvially sculpted bedrock terrace at the modern river level (site 6a; Table 2). Except for ^{10}Be in one sample, blank-corrected ^{10}Be and ^{26}Al concentrations are within error of zero; ^{26}Al concentrations are $\leq 3\%$ of those measured on other surfaces and are therefore negligible. The steady-state erosion rate on this surface calculated from the error-weighted average age is 2.7 m/ka, but values > 10 m/ka are permitted by the uncertainty in this age.

The seasonal high discharge is marked by a stain line 10–230 m above the surface of the Indus River in the MG during low flow, indicating that surfaces

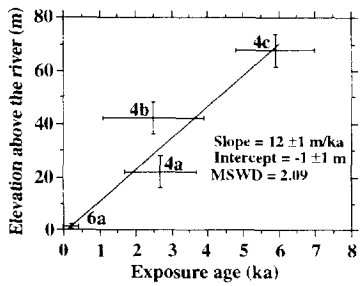

Fig. 3. Distribution of weighted mean exposure ages of a sloping, fluvially sculpted valley wall (site 4) and of a terrace in the modern riverbed (site 6a). An error-weighted regression suggests that stream erosion of strath surfaces is insignificant above the level of the river at low discharge.

well above the low-discharge river level may be undergoing some fluvial erosion. To test the vertical extent of fluvial erosion above the river, a sloping, fluvially sculpted valley wall at site 4 was sampled at three levels above the low-flow river (22, 42, and 65–70 m). The weighted mean of ages from both ^{26}Al and ^{10}Be increase with elevation (Fig. 3) and show that fluvial erosion of surfaces more than 20 m above the low-flow Indus River is likely to be negligible. This result is consistent with the expectation that the bulk of mechanical erosion occurs in contact with the portions of the flow where sediment is concentrated, such as near at the base of the stream channel [14]. However, the scatter in the correlation between elevation and age is also permissive of the interpretation data support only a weak linear correlation, suggesting that surfaces 20 m apart in elevation may be fluvially eroded roughly simultaneously.

4.3. Exposure ages of strath surfaces and their distribution

4.3.1. Evaluation of multiple ages on strath surfaces

Each of the surfaces > 100 m above the river yields a range in ages. The different ages are difficult to explain using the cosmogenic nuclide data alone; the ^{26}Al and ^{10}Be ages of most samples are concordant within 2σ (Table 2; [8]). However, there is no reasonable mechanism for enriching samples in both ^{10}Be and ^{26}Al with respect to other samples from the same surface and field observations provide evidence of differential erosion or shielding that accounts for the younger exposure ages on these sites.

Differential shielding and/or erosion likely explains the multiple ages at sites 1, 2, 6b, and 10 (Table 2). The samples yielding the older exposure ages were obtained from the tops of bedrock knobs exposed to the wind or from dipping surfaces (> 20°) that might have prevented significant debris cover. Younger exposure ages were obtained from more flat-lying portions of the straths where intermittent cover could have reduced exposure ages. At site 2, the sample yielding the youngest age is from a flat hackly surface 3 m below the well preserved, fluvially polished knob on which we collected the two older samples. Post-abandonment burial, combined with visual evidence of ~ 5 cm of post-abandonment erosion of this flat surface could account for the young age of the quartz vein relative to the older ages of samples collected from the wind-swept knob. Younger ages were also obtained from the flatter surfaces on sites 1, 2, 6b, and 10, so the older exposure ages from more steeply dipping surfaces likely represent the best estimates of the time of abandonment of those sites.

Of the two ages at site 5, the older age is probably more reliable because the sample that yields the younger age was collected from a loose block. The surface at site 5 did not preserve the finer fluvial features observed on lower straths and the older exposure age, 32 ka, is strikingly young for this 410 m high strath compared to lower, nearby straths, especially site 6b immediately below. If the 32 ka age at site 5 is the true abandonment age, then either fluvial incision to strath 6b (255 m below site 5) was very rapid or the 27 ka age for site 6b is an overestimate. However, as indicated above, we favor the older rather than the younger (cf. [5]) age on strath 6b because burial or erosion could account for the younger exposure ages. Hence, the 32 ka exposure age on site 5 is probably the result of erosion and/or burial and underestimates the true age of abandonment of this surface. This site will not be considered further here.

4.3.2. *Distribution of strath exposure ages in the study area*

Fig. 4 shows the average exposure age and height distribution of sampled straths along the Indus River. Average strath ages (Table 2) are error-weighted and exclude younger ages based upon the criteria discussed in the preceding section. This approach leads to preferred ages that differ from those previously reported [5], notably for site 6b (formerly site 6). Ages range from 0.2 to 65.0 ka and, in general, increase with increasing elevation above the river. In three cases, site 1 compared with site 2, site 4a versus site 4b, and the two samples from site 8, surfaces separated by 20–37 m in elevation yield younger or similar or even reversed exposure ages. Post-abandonment erosion or burial of site 1 likely lowered the exposure age relative to site 2, as discussed above. At sites 4a and 4b and site 8, the similarity in age between surfaces 20–28 m apart might be the product of simultaneous formation. Alternatively, the differences in calculated exposure ages may indicate that it is difficult to resolve differences in ages between straths separated by only 20 m with these data. Because burial or erosion might have reduced the apparent exposure ages on the higher surfaces, we emphasize the age of the lower, older surface in our interpretations.

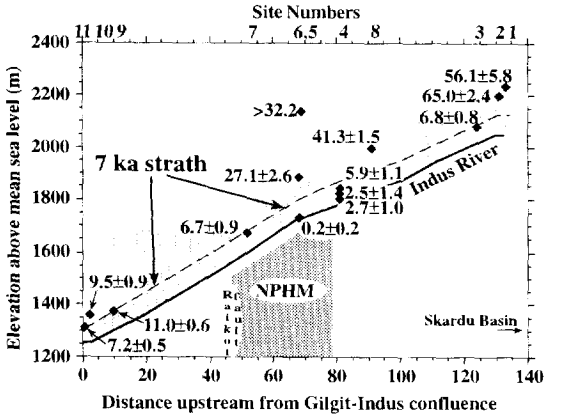

Fig. 4. Elevations (a.s.l.) and average exposure ages (excluding italicized data in Table 2) of straths shown with respect to the distance upstream along the Indus River from its confluence with the Gilgit River. Reported errors are 2σ. The heavy line shows the smoothed longitudinal profile of the Indus River. The dashed line is an extrapolation of a hypothetical 7 ka strath level based on four different sites spanning the study area. The shaded areas above the river show the range of possible altitudes of the Indus River channel at around 7 ka and are delimited by the maximum and minimum possible gradients of the Indus River at 7 ka. For site 9, it is possible that incision to the present river level occurred 7 ka ago. Exposure ages for straths between 145 and 192 m (1, 2, 8, and 6b) above the present river elevation decrease downstream, with the youngest age found within the rapidly exhuming NPHM.

Four low strath sites appear to define a 7 ka strath level that extends throughout the MG and which varies between 65 and 80 m in elevation above the river (Fig. 4). The proposed strath level is drawn roughly parallel to the modern river and projected to 7 ka based on the incision rates at each of the four sites. Site 9, located near the Gilgit–Indus River confluence, occurs at the height of the proposed 7 ka strath level but has an exposure age of 11 ka. Field evidence suggests that cutting of this terrace was followed by incision to about the present base level, fill over the level of the terrace, and reincision through the fill to the present base level. Thus, the river level at this site has been highly variable and the incision rate calculated from this age is likely a minimum (Fig. 5). It is possible that the profile of the Indus River was different than it is today; in Fig. 4, the lower and upper limits of the grey boxes constrain the minimum and maximum possible heights of the river at 7 ka with respect to its present altitude. However, the sites with exposure ages < 10 ka are distributed throughout the MG and interpolation between them does not require the profile to have changed much over at least the last 7 ka.

The high straths, 1, 2, 6b and 8, are located at about the same level (145–192 m) above the modern river (Fig. 4) but the exposure ages progressively increase upstream, from 27 ka at site 6b in the NPHM to 65 ka at site 2 near the Skardu Basin. If the difference in age and cosmogenic nuclide concentrations between site 6b and 2 were due solely to post-abandonment erosion of the strath surface at site 6b, the difference would require a loss of 0.33 m of the original surface at a rate of 0.005 m/ka, assuming constant erosion [9]. This amount of erosion is difficult to reconcile with the very good preservation of fluvial features at site 6b. Furthermore, the upstream progression from younger to older exposure ages on the high straths argues against the fortuitous circumstances required for burial to have produced this pattern. Thus, the age difference between the high straths near the Skardu Basin and those to the west likely reflects real differences in abandonment ages.

4.4. Bedrock incision rates

With the addition of new data presented here, it is possible to obtain a more detailed record of fluvial incision than described in [5] and gain new insights into the recent history of incision in the MG. Two sets of incision rates are calculated, one for the lower, 7 ka straths and one for the older, higher straths (Fig. 5). Incision rates for the lower straths are the quotients of the differences in exposure age and height above the low-flow river level. This calculation assumes that no significant erosion occurs above the surface of the river at low flow. If it is assumed that erosion extends 10–20 m above the low-flow level [5], rates would be reduced by ~ 15–30%. The low straths give fast bedrock incision rates which show a modest increase between points upstream (9.6 m/ka) and the NPHM (11.9 m/ka). Incision rates at the confluence are also fast but are slower at site 9 because of the complex exposure history of this site.

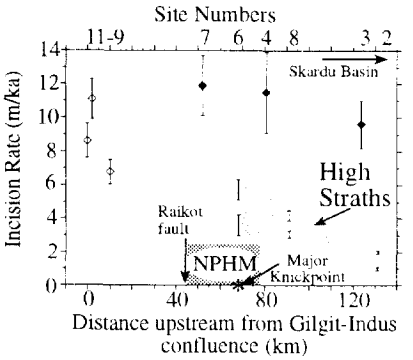

Fig. 5. The geographical distribution of incision rates for both the older, higher straths (27–65 ka) and the lower, younger straths (< 7 ka) within the MG show a persistent downstream increase of 1–3 m/ka nearing the Raikot fault. Errors are 2σ and include uncertainties in strath height. The increase likely reflects the differential bedrock uplift rate between the NPHM and the Skardu Basin. Incision rates for the high straths are given as a range within the shaded area where the minimum rates are the quotient of the difference in exposure age and the difference in height above the river of adjacent high and low straths, and the maximum possible rates are based on the age and height difference between the strath and the lowest possible altitude of the Indus at 7 ka (Fig. 4). These maximum incision rates are slower than those previously reported for the high straths [5]. The very fast incision rates for low straths in the MG (♦) and low straths at the confluence (◇) are the quotient of strath height above the river and exposure age. The temporal increase in incision rates in the MG likely reflects an increase in discharge since 15 ka. Rapid incision rates for Holocene age straths at the confluence are consistent with the rapid incision rates of the < 7 ka straths in the MG despite changes in the controls on incision rates at the confluence.

Minimum incision rates for the high straths are given as the differences between the ages and heights above the river of adjacent high and low straths. A minimum incision rate of 0 m/ka for the high straths seems unlikely because it requires the highly stepped, maximum altitude 7 ka longitudinal profile to pertain (Fig. 4) and unrealistically fast incision rates of > 20 m/ka would have to apply at each step in this profile. Maximum incision rates are based on the difference in altitude between the high straths and the minimum 7 ka altitude of the Indus River below the high strath sites (Fig. 4). The differences between maximum and minimum incision rates range from 35% to 58%. Because they do not compound the higher incision rates of the younger terraces, these analyses yield incision rates for the high straths that are slower than those presented by [5]. Despite this, these data define a downstream increase in bedrock incision rates between the Skardu Basin and the NPHM within the MG between 65 and 27 ka (Fig. 5). Notably, the absolute difference in incision rate for the high straths, 1–3 m/ka, is about the same as that for the low straths, although there is greater uncertainty in the differential incision rate for the low straths. The occurrence of faster incision rates closer to the Raikot fault zone suggests that the Indus River has been responding to localized bedrock uplift by incising more rapidly near the locus of neotectonic activity.

The difference in the magnitude of the bedrock incision rates between the high and low straths indicates that an acceleration in incision rates in the MG must have occurred in the past 27 ka. Reference to a hypothetical 27 ka strath level (Fig. 6A) extrapolated from the low straths' incision rates shows that these fast incision rates could not have persisted for this long: the hypothetical paleo-profile is above dated straths with older exposure ages. One limit on the time at which incision rates in the MG increased can be obtained by dividing the height of the high straths by the incision rates of nearby low straths: this assume an instantaneous acceleration of incision rates from negligible to those of the low straths. Resulting ages for this step-wise increase in incision rates are 13–15 ka (Fig. 6A). If it is assumed that the incision rate for the high straths in the NPHM was at least the differential incision rate in the MG, ~ 2 m/ka, a step-wise increase in incision rates to values ob-

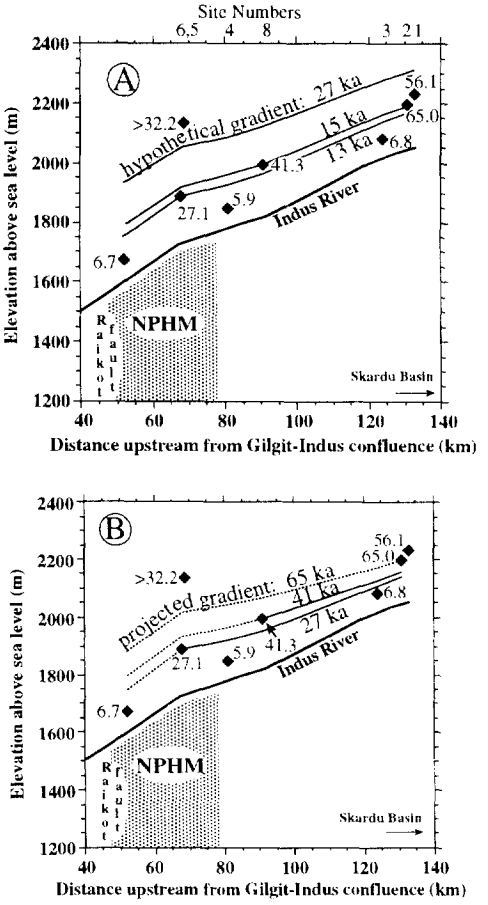

Fig. 6. Paleogradients projected from incision rates (Fig. 5) for (A) the low straths and (B) the high straths (using slower rates) and compared to strath ages and elevations; lines are dashed where projections are less certain. In (A) the hypothetical 27 ka strath level passes above actual strath sites with exposure ages ≤ 27 ka, showing that the rapid incision rates of the low straths could not have persisted for the last 27 ka. The 13 and 15 ka contours bracket the elevations of the higher straths and help constrain the upper limit of the onset of rapid incision in the MG. In (B) the shallowing of the paleogradient indicated by these projections implies smaller changes in stream power downstream than pertain today, a situation that is inconsistent with the observed downstream increases in incision rates for the high straths. Uplift of the NPHM relative to points upstream explains the downstream distortion in the projected isochronous strath levels and the downstream increase in incision rates.

tained from the low straths could not have occurred before 10 ka. If incision rates increased continuously from 65 ka to the present, the large amount of incision occurring in < 7 ka (65–80 m) requires that the largest incision rate increases occur in the last 25

ka. While these scenarios are only approximations to the more gradual changes in incision rates that probably pertain, it is likely that the largest incision rate increases occurred near the end of or after the last global glacial maximum (15–25 ka; [15,16]).

5. Discussion

The results presented above show that bedrock incision rates in the MG are fast enough to preclude the ingrowth of cosmogenic nuclides prior to strath abandonment. The changes observed in bedrock incision rates in the MG reveal both spatial and temporal patterns not previously recognized (cf. [5]). The rates of bedrock incision calculated from the ages and elevation of abandoned straths: (1) increase 1–3 m/ka downstream between the Skardu Basin and the NPHM and (2) at least doubled throughout the MG some time in the past 15 ka. Notably, the increase in incision rates, previously attributed to differential uplift along an unknown structure [5] between sites 2 and 3 near the Skardu Basin is best explained as an acceleration in incision rates between 7 and 18 ka ago (Fig. 6A). The bedrock incision rates we calculate for the late Pleistocene and Holocene Indus River are fast. They are not unprecedented, however, and are comparable to peak bedrock incision rates of 7 m/ka on the Dearborn River in Montana, USA, for two glacial periods [1].

The following section explores the linkages between apparent downstream bedrock uplift and the observed spatial pattern in the incision rates based on a qualitative analysis of the dominant controls on bedrock incision along the Indus River. Strath ages and apatite fission track ages are also compared and used to constrain differential bedrock uplift rates back to 1 Ma. Finally, the temporal increase in incision rates is compared with the controls on bedrock incision in the MG and attributed to climatic change.

5.1. Controls on incision rates

Bedrock incision rates are likely a function of stream power: a quantifiable physical description of the total power of flowing water [17] that constrains the rate at which a stream can do work to erode its channel. Incision occurs due to the processes of lowering due to knickpoint propagation, stream power, abrasion by rock fragments moving in the river, flow cavitation, dissolution, and debris flow scour [18,19]. Knickpoint propagation is an important mechanism for channel incision that primarily depends upon the physical characteristics of the rock flooring the stream channel [18]. Abrasion and flow cavitation are important processes in the erosion of the Indus River channel and ultimately depend upon stream power. Dissolution of the bedrock in the MG probably occurs at a rate well below the rate of mechanical erosion. Debris flow scour can produce the bulk of mechanical stream channel erosion in a very short period, but likely operates on very steep, low-order channels [18]. Debris flow scour might be important along short stretches of the MG immediately after landslides blocking the Indus River had been catastrophically breached; thus, to the first order, differential erosion of the Indus River's bedrock channel is treated as a function of knickpoint propagation and specific stream power.

A major knickpoint occurs in the Indus River near the eastern side of the NPHM (Fig. 4). The formation and propagation of knickpoints are controlled by gradients of tributaries at confluences, the structural fabric of the bedrock, differential rock resistance, changes in base level, differential bedrock uplift, and the local slope of the river bottom [2,18,20]. The knickpoints of many major Himalayan rivers occur where the rivers flow across tectonically active structures [21]. In the MG, the knickpoint occurs about 30 km upstream from, and in the hanging wall of, the active Raikot fault, an oblique, upstream-dipping reverse fault. A likely explanation for the change in the Indus River gradient is, therefore, that bedrock uplift along the Raikot fault zone within the NPHM causes a base level fall west of the NPHM and generates a knickpoint which propagates upstream [18]. A change in mineral foliation, from upstream-dipping to downstream-dipping mineral foliations in gneissic rocks [22], also occurs approximately 10 km downstream from the knickpoint in the MG (cf. [20]). However, it is unlikely that the region of steep gradient within the NPHM is caused solely by a change in the dip direction of the bedrock foliation.

Steeper downstream slopes and narrower river widths within the NPHM cause downstream in-

creases in specific stream power. Specific stream power is the product of discharge, fluid density, gradient, and acceleration due to gravity divided by channel width [17]. Of these variables, only gradient and river width vary significantly today between the Skardu Basin and the confluence of the Gilgit and Indus rivers (sites 1–9). At the major knickpoint near the eastern side of the NPHM, the average river gradient steepens downstream to 7 m/km from about 5 m/km upstream [5] and the river appears to narrow by no more than 20%, which translates into a 75% increase in stream power. If the relationship between stream power and the rate of bedrock incision is proportional (cf. [4,23]), incision rate increases in the MG should be proportional to increases in stream gradient. The 28% increase in Holocene incision rates across the major knickpoint in the MG, obtained from the low straths (Fig. 5), is the same order of magnitude as comparable to this inferred increase in stream power across the major knickpoint in the MG. Thus, gradient-related variations in stream power appear sufficient to explain the pattern of Holocene incision rates.

A gradient-related variation in stream power alone cannot account for the pattern of incision rates displayed by the high straths: projected paleo-gradients (Fig. 6B) are significantly flatter than would be inferred from the more than 200% proportional change in incision rates between upstream and downstream straths. Instead, a 1–3 m/ka difference in high strath incision rates appears to be imposed upon the Indus River by the differential rate of bedrock uplift between the NPHM and the upper MG. Persistent downstream bedrock uplift with no differential rate of incision would cause the Indus River to aggrade upstream of the NPHM and to form a long reach with an untenably high gradient within the NPHM, whereas the current longitudinal profile of the Indus River in the MG is probably a dynamic equilibrium form (cf. [2]) that has been maintained by a powerful river responding to bedrock uplift of its channel within the NPHM [5].

5.2. *Incision and bedrock uplift in the MG of the Indus River*

The NPHM is characterized by extreme topographic relief, exposures of lower-plate basement gneisses, and very young apatite fission track ages that correspond to high exhumation rates (Fig. 1B; [7]), strongly suggesting that this area is experiencing rapid bedrock uplift with respect to the surrounding terrane. Bedrock uplift associated with reverse motion on the Raikot fault best explains the persistently faster incision rates of the Indus River in the NPHM relative to the upper MG. That the difference in incision rates persists despite the large increase in incision rates sometime in the past 15 ka suggests that the relative bedrock uplift rates may not have changed much in the last 65 ka. Assuming that the late Pleistocene longitudinal profile of the MG was similar to the modern gradient, the 1–3 m/ka difference in incision rates delimits the maximum rate of bedrock uplift of the NPHM relative to points upstream for at least the last 65 ka.

The downstream younging of apatite fission track ages in the MG (Fig. 1B) reflects a greater rate of exhumation in the NPHM than in the upper MG. The difference in exhumation rates should be comparable to the difference in incision rates, if the differential exhumation rate is equivalent to the differential bedrock uplift rate. Estimates of the absolute difference in exhumation rates depend on the geothermal gradients used and would be 7.5 m/ka for 35°C/km and 2.9 m/ka for 90°C/km (Fig. 1B); these assume a 150°C annealing temperature for apatite [24] and a laterally uniform geothermal gradient. Near-surface geothermal gradient estimates for the Nanga Parbat massif vary from 60°C/km [25–27] to > 100°C/km [28], although the thermal models [28] with the highest estimates imply a spatial distribution of exhumation rates calculated from apatite fission track ages [7] that is inconsistent with the pattern of uplift assumed in the model. However, relatively steep geothermal gradients that shallow away from the NPHM might be anticipated from the advection of isotherms toward the surface that would result from rapid unroofing in this area [28,29]. Proposing a model for the spatial variability of the geotherm between the NPHM and the Skardu Basin is beyond the scope of this paper but the difference in incision rates sets an upper limit on the differential bedrock uplift rate between the NPHM and the Skardu Basin over the last 65 ka. A differential incision rate of 3 m/ka that has persisted over the last 0.5 Ma is consistent with a differential exhumation rate of 3–4

m/ka, resulting from a near-surface geothermal gradient that varies from $\leq$ 80–90°C/km in the NPHM to 35°C/km in the Skardu Basin. If the differential incision rate is the same as the differential exhumation rate, bedrock uplift of the Indus River channel is required to maintain a reasonable longitudinal profile [5].

5.3. Temporal increase in incision rate

In addition to evidence for differential incision of the MG, our data provide evidence for a large, 6–8 m/ky increase in incision rates throughout the MG within the last 15–20 ka (Fig. 5). This increase was likely caused by an increase in stream power. Holding all other variables of stream power constant during this time period results in an unrealistically large change in gradient if stream power is proportional to bedrock incision rates (e.g., [4]). An increase in discharge and/or change in sediment load best explains the increase in incision rates and might have been associated with deglaciation of the Karakoram Mountains and Deosai plateau. The upper limit on the timing of this increase is well after the 30–65 ka age range of dated glacial features associated with the last extensive glacial episode in the Karakoram [30,31], yet it overlaps the end of the last global glacial maximum. This apparent diachronism (cf. [1]) appears to parallel other evidence for differential response of alpine glaciers and continental ice sheets to global climate change [32]. If the large increase in incision rates since 15 ka was the result of increased discharge, it would have affected the entire Indus River. The fast incision rates at the Gilgit–Indus River confluence (straths 10 and 11) support this hypothesis.

6. Conclusions

We have demonstrated the potential of in situ cosmogenic ^{10}Be and ^{26}Al exposure age dating of bedrock straths for determining variations in bedrock incision rates. The results show decisively that straths in the MG formed quickly, that their exposure ages should closely approximate their abandonment age, and that incision rates are faster in the Nanga Parbat–Haramosh massif (NPHM) than in the upper Middle Gorge (MG). The 1–3 m/ka difference between incision rates in the NPHM and upper MG must reflect the maximum relative bedrock uplift rate for the NPHM. Bedrock uplift of the river channel near the Raikot fault creates a migrating knickpoint and region of steep gradient within the NPHM; for the younger straths we have shown that the gradient-related increase in stream power is accompanied by a proportional increase in incision rate. The differences in exhumation rates and incision rates between the NPHM and upper MG are broadly similar if the geotherm in the NPHM is steep and suggest that differential bedrock uplift of 1–3 m/ka has persisted for the last 0.5 Ma. A 6–8 m/ka increase in incision rates in the last 15 ka may be linked to deglaciation of the MG's watershed or other climatically modulated increases in stream or sediment discharges within the MG's watershed.

Acknowledgements

We thank R.S. Anderson, S. Anderson, N. Brozovic, and J. Vergés for their assistance and discussions in the field and R.S. Anderson for his contributions to the development of this project. J.W. Kirchner and an anonymous reviewer made thoughtful contributions to the text. J. Southon provided much assistance in obtaining the AMS analyses and J. Koning and G. Littman assisted with laboratory work. This work was supported by NSF grant EAR9219852 to MRR and DWB, a grant from the Lawrence Livermore National Laboratory Institute of Geophysics and Planetary Physics to MRR, MC, and RF, and a GSA student grant #5191-93 to JL. *[AC]*

References

[1] M.G. Foley, Quaternary diversion and incision, Dearborn River, Montana, GSA Bull. 91 (II) (1980) 2152–2188.
[2] D.J. Merritts, K.R. Vincent, E.E. Wohl, Long river profiles, tectonism, and eustasy: A guide to interpreting fluvial terraces, J. Geophys. Res. 99 (B7) (1994) 14031–14050.
[3] S.F. Personius, Late Quaternary stream incision and uplift in the forearc of the Cascadia subduction zone, western Oregon, J. Geophys. Res. 100 (B10) (1995) 20193–20210.
[4] R.S. Anderson, Evolution of the Santa Cruz Mountains, California, through tectonic growth and geomorphic decay, J. Geophys. Res. 99 (B10) (1994) 20161–20179.

[5] D.W. Burbank, J. Leland, E. Fielding, R.S. Anderson, N. Brozovic, M.R. Reid, C. Duncan, Bedrock incision, rock uplift and threshold hillslopes in the northwestern Himalayas, Nature 379 (1996) 505–510.

[6] R.W.H. Butler, D.J. Prior, R.J. Knipe, Neotectonics of the Nanga Parbat Syntaxis, Pakistan, and crustal stacking in the northwest Himalayas, Earth Planet. Sci. Lett. 94 (1989) 329–343.

[7] P.K. Zeitler, Cooling history of the NW Himalaya, Pakistan, Tectonics 4 (1) (1985) 127–151.

[8] K. Nishiizumi, E.L. Winterer, C.P. Kohl, J. Klein, R. Middleton, D. Lal, J.R. Arnold, Cosmic ray production rates of ^{10}Be and ^{26}Al in quartz from glacially polished rocks, J. Geophys. Res. 94 (B12) (1989) 17907–17915.

[9] D. Lal, Cosmic ray labeling of erosion surfaces: in situ nuclide production rates and erosion, Earth Planet. Sci. Lett. 104 (1991) 424–439.

[10] C.P. Kohl, K. Nishiizumi, Chemical isolation of quartz for measurement of in-situ-produced cosmogenic nuclides, Geochim. Cosmochim. Acta 56 (1992) 3533–3587.

[11] D.H. Clark, P.R. Bierman, P. Larsen, Improving in situ cosmogenic chronometers, Quat. Res. 44 (1995) 367–377.

[12] K. Nishiizumi, C.P. Kohl, E.M. Shoemaker, J.R. Arnold, J. Klein, D. Fink, R. Middleton, In situ ^{10}Be–^{26}Al exposure ages at Meteor Crater, Arizona, Geochim. Cosmochim. Acta 55 (1991) 2699–2703.

[13] S.R. Sutton, Thermoluminescence measurements on shock-metamorphosed sandstone and dolomite from Meteor Crater, Arizona 1. Thermoluminescence of Meteor Crater, J. Geophys. Res. 90 (1985) 3690–3700.

[14] R.G. Shepherd, S.A. Schumm, Experimental study of river incision, Geol. Soc. Am. Bull. 85 (1974) 257–268.

[15] N.J. Shackleton, Oxygen isotopes, ice volume, and sea level, Quat. Sci. Rev. 6 (1987) 183–190.

[16] E. Bard, B. Hamelin, R.G. Fairbanks, A. Zindler, Calibration of the ^{14}C timescale over the past 30,000 years using mass spectrometric U–Th ages from Barbados corals, Nature 345 (1990) 405–410.

[17] R.A. Bagnold, An approach to the sediment transport problem from general physics, USGS, Washington, D.C., 1966.

[18] M.A. Seidl, W.E. Dietrich, The problem of channel erosion into bedrock, in: K.-H. Schmidt, J.D. Ploey (Eds.), Functional Geomorphology, 23, Catena, Cremlingen, 1992, pp. 101–124.

[19] M.A. Seidl, W.E. Dietrich, J.W. Kirchner, Longitudinal profile development into bedrock: An analysis of Hawaiian channels, J. Geol. 102 (1994) 457–474.

[20] J.R. Miller, The influence of bedrock geology on knickpoint development and channel-bed degradation along downcutting streams in South-Central Indiana, J. Geol. 99 (1991) 591–605.

[21] L. Seeber, V. Gornitz, River profiles along the Himalayan arc as indicators of active tectonics, Tectonophysics 92 (1983) 335–367.

[22] M.P. Searle, Geology and Tectonics of the Karakoram Mountains, Wiley, Chichester, UK, 1991, 358 pp.

[23] N.A. Rosenbloom, R.S. Anderson, Hillslope and channel evolution in a marine terraced landscape Santa Cruz, California, J. Geophys. Res. 99 (B7) (1994) 14013–14029.

[24] N.D. Naeser, C.W. Naeser, T.H. McCulloh, The application of fission track dating to the depositional and thermal history of rocks in sedimentary basins, in: N.D. Naeser, T.H. McCulloh (Eds.), Thermal History of Sedimentary Basins: Methods and Case Studies, Springer, New York, 1989, pp. 157–180.

[25] D.M. Winslow, P.K. Zeitler, C.P. Chamberlain, L.S. Hollister, Direct evidence for a steep geotherm under conditions of rapid denudation, Western Himalaya, Pakistan, Geology 22 (1994) 1075–1078.

[26] D.M. Winslow, C.P. Chamberlain, P.K. Zeitler, Metamorphism and melting of the lithosphere due to rapid denudation, Nanga Parbat Massif, Himalaya, J. Geol. 103 (1995) 395–409.

[27] P.K. Zeitler, C.P. Chamberlain, H.A. Smith, Synchronous anatexis, metamorphism, and rapid denudation at Nanga Parbat (Pakistan Himalaya), Geology 21 (1993) 347–350.

[28] D. Craw, P.O. Koons, D. Winslow, C.P. Chamberlin, P. Zeitler, Boiling fluids in a region of rapid uplift, Nanga Parbat Massif, Pakistan, Earth Planet. Sci. Lett. 128 (1994) 169–182.

[29] K. StŸuwe, L. White, R. Brown, The influence of eroding topography on steady-state isotherms. Application to fission track analysis, Earth Planet. Sci. Lett. 124 (1994) 63–74.

[30] J.F. Shroder Jr., M.S. Khan, R.D. Lawrence, I.P. Madin, S.M. Higgins, Quaternary glacial chronology and neotectonics in the Himalaya of northern Pakistan, Spec. Pap. Geol. Soc. Am. 232 (1989) 275–294.

[31] L.A. Owen, Terraces, uplift and climate in the Karakoram Mountains, northern Pakistan: Karakoram intermontane basin evolution, Z. Geomorph. N.F. Suppl. 76 (1989) 117–146.

[32] A. Gillespie, P. Molnar, Asynchronous maximum advances of mountain and continental glaciers, Rev. Geophys. 33 (1995) 311–364.

[33] A. Pêcher, P.L. Fort, Is Nanga Parbat an active indenter or a passive dome?, in: 11th Himalaya–Karakorum–Tibet Workshop, Northern Arizona University, Flagstaff, AZ, 1996, pp. 11–14.

[34] D.R. Lide, H.P.R. Frederikse, CRC Handbook of Chemistry and Physics, CRC Press, Boca Raton, Fla., 1996.